International Journal of Environmental Science and Technology
https://doi.org/10.1007/s13762-020-03074-4

ORIGINAL PAPER

A comparative study of different materials (drinking water treatment sludge, nanoclay, and modified nanoclay) for simultaneous removal of hexavalent chromium and lead

A. Heidari[1] · M. H. Sayadi[2,3] · Z. Biglari Quchan Atigh[1]

Received: 13 June 2020 / Revised: 6 November 2020 / Accepted: 8 December 2020

Abstract

Drinking water treatment sludge in large quantities was generated in the flocculation process of the treatment plant, all over the world. It considered the secondary raw material due to having valuable inorganic compounds such as iron. Herein, a novel green method was developed to recover iron from drinking water treatment sludge for synthesizing nanoscale iron supported on nanoclay by a lemon Beebrush polyphenol. The surface of nanoclay containing iron nanoparticles was modified with ethylenediamine for their applications as heavy metals adsorbent. The field emission scanning electron microscopy, energy-dispersive x-ray spectroscopy, thermogravimetric analysis, derivative thermogravimetry, and Fourier-transform infrared spectroscopy techniques were utilized to examine the adsorbents. Based on the results of energy-dispersive X-ray analysis, iron and nitrogen were successfully introduced into the structure of modified nanoclay. A batch adsorption system was used to investigate the simultaneous removal performance of hexavalent chromium and lead onto drinking water treatment sludge, nanoclay, and nanoclay-iron nanoparticle-ethylenediamine. The influence of factors, e.g., initial concentration, contact time, pH, adsorbent dosage, and temperature, were evaluated. The maximum uptake for chromium was 0.303, 0.352, and 0.984 mmol/g and for lead 0.03, 0.042, and 0.108 mmol/g at pH of 3 onto drinking water treatment sludge, nanoclay, and nanoclay-iron nanoparticle-ethylenediamine, respectively. The results show that the quantity of chromium and lead adsorbed onto modified nanoclay was more than 2.5-fold than that adsorbed onto unmodified nanoclay. The equilibrium adsorption data of hexavalent chromium and lead were fitted well with the Langmuir isotherm model ($R^2 > 0.97$). Besides, the pseudo-second-order kinetic model demonstrated the kinetic adsorption of the metal ions. The thermodynamic constants suggested that the adsorption of lead by three adsorbents was exothermic and spontaneous while that of hexavalent chromium was endothermic. It leads to a finding that nanoclay-iron nanoparticle-ethylenediamine could be an effective adsorbent for heavy metals removal from water and wastewater.

Keywords Adsorption kinetics · Drinking water treatment sludge · Heavy metals · Isothermal models · Zero-valent iron nanoparticles

Editorial responsibility: Samareh Mirkia.

Supplementary material The online version of this article (https://doi.org/10.1007/s13762-020-03074-4) contains supplementary material, which is available to authorized users.

✉ A. Heidari
heidari@um.ac.ir

[1] Department of Environmental Science, Faculty of Natural Resources and Environment, Ferdowsi University of Mashhad, Mashhad, Iran

[2] Department of Environmental Engineering, Faculty of Natural Resources and Environment, University of Birjand, Birjand, Iran

[3] Department of Environmental Engineering, Faculty of Agriculture and Natural Resources, Ardakan University, Ardakan, Iran

Published online: 26 February 2021

Introduction

Among all the pollutants, heavy metals are paramount due to their toxic nature and their risk of accumulation in living organisms through food chains (Sarı et al. 2007). For example, hexavalent chromium (Cr(VI)) and lead (Pb(II)) are very toxic heavy metals, with the maximum permissible quantity of 0.05 mg/L in potable water, according to Environmental Protection Agency (EPA) (Gupta et al. 2016; He et al. 2017; Sharma et al. 2018). Pb(II) can create severe threats to human health, including damages to the nervous and immune systems (Gupta et al. 2016; Şölener et al. 2008). Adverse health problems related to Cr(VI) exposure consist of nasal and skin irritation, eardrum perforation, and lung carcinogen (Karthik et al. 2017). Therefore, the removal of heavy metals before releasing them into the media is needed. Some water treatment methods, for example, ion exchange, reverse osmosis, membrane separation, coagulation and flocculation, chemical sedimentation, and adsorption, have been used for heavy metals removal (Bolisetty et al. 2019; Gupta et al. 2016; Karthik et al. 2017; Sharma et al. 2018). However, adsorption by different materials is an emerging alternative method because of relatively cost-effective, simplicity of design and operation, removal at low concentrations, low sludge production, and environmental friendly (Foo and Hameed 2010; Gupta et al. 2016; Sharma et al. 2018; Sis and Uysal 2014). Based on the profits of adsorption, the development of a new adsorbent with properties and characteristics that indicate a high adsorption capacity for metal ions is necessary. Therefore, relatively inexpensive and readily accessible raw materials such as drinking water treatment sludge (DWTS) and clay should be investigated to synthesize appropriate adsorbents for the removal of Cr(VI) and Pb(II) from water.

DWTS is a by-product made in the potable water treatment plant, mainly generated in the coagulation and flocculation process in the sedimentation basin. A typical treatment plant generates 100.000 metric tons of residue annually worldwide (Ahmad et al. 2016). Currently, the literature estimates overall DWTS production up to several million tons each year (Evuti and Lawal 2011; Zhou et al. 2018). DWTS is regarded as a waste, usually landfilled or discharged directly into the environment (Zhao et al. 2011). Clay, humus, and coagulant were the significant constituents of DWTS (Meng et al. 2016). It contains relatively high quantities of chemical elements such as iron (Fe), aluminum (Al), and silicon (Si) that predominantly arise from the flocculants applied in water purification, quality of raw water, and treatment technology (Ahmad et al. 2016). Until now, worthy attempts have been made that identified and explored the conversion of DWTS to useful materials [e.g., coagulant Keeley et al. 2014), adsorbent (Bian et al. 2019; Jiao et al. 2017), cement (Frías et al. 2014), brick and ceramic (da Silva et al. 2015)]. Recently, recycling of metals such as Al, Si, and Fe from treatment sludge to synthesis non-crystalline nanomaterials have been reported (Meng et al. 2016; Zou et al. 2012, 2013). The magnetic particle was prepared from iron oxides extracted from DWTS via hydrothermal or calcination techniques with the addition of different reductant agents, including glycol (Zhu et al. 2015), ascorbic acid 72 (Zhu et al. 2018b), and ethylene glycol (Meng et al. 2016). A green technique should be developed for DWTS recycling to attain sustainability.

Recently, the zero-valent iron nanoparticle has been revealed to be a sound absorbent for heavy metals removal due to high reduction reactivity, high surface energy, other reactive surface sites, and considerable reaction rate. Nevertheless, some practical challenges, including reduced mobility, dispersivity, and durability because of its aggregation, chemical instability, and the tendency for oxidization, restricted its use in environmental remediation. Therefore, to solve these issues, iron nanoparticles immobilized on some support materials such as bentonite (Shi et al. 2011), montmorillonite (Zhang et al. 2013), kaolinite (Zhang et al. 2011), zeolite (Kim et al. 2013), and rectorite (Luo et al. 2013).

In this study, the primary purpose was to examine the green synthesis of iron nanoparticle from iron extracted from DWTS instead of synthetic iron using a lemon Beebrush extract as a reductant supported on nanoclay. Nanoclay was prepared from clay fraction of bentonite, and subsequently, functionalized with ethylenediamine. Ethylenediamine is an organic compound with low-toxicity, low-cost, and comprises two functional amine groups, which can create stable complexes with metal ions. Therefore, grafting ethylenediamine to NC may enhance its adsorption ability and need to be investigated. Recently, Bello et al. (2019) have reported the preparation of iron nanoparticle from DWTS by the $NaBH_4$ reduction method as a conjugate with kaolin. However, this work used the chemical method for iron nanoparticle synthesis and, like other studies, immobilized it in bulk clay materials (Kim et al. 2013; Shi et al. 2011). Besides, the prior works confirmed that the iron nanoparticle synthesis in the attendance of clay minerals reduces their aggregation (Abbassi et al. 2013; Tandon et al. 2013). To the best of our knowledge, there is no study examining both green syntheses of iron nanoscale from DWTS supported on ethylenediamine grafted nanoclay and the application of its composite for Cr(VI) and Pb(II) removal. The secondary objective was to assess and compare the performance of DWTS, nanoclay (NC), and nanoclay-Fe nanoparticle-ethylenediamine (NCFN) to adsorb Cr(VI) and Pb(II) from an aqueous solution. The influence of various adsorption factors (pH, initial metal concentration, contact time, and

adsorbent dosage) was investigated. The abovementioned metal ions adsorption mechanisms were determined through isotherm, kinetic, and thermodynamic studies. This research was performed during October 2018–September 2019 at the Ferdowsi University of Mashhad, Mashhad, Iran.

Materials and method

Materials

The bentonite sample was purchased from Zarin Khak Company, a mine located in Ghayen, South Khorasan, Iran. The DWTS was obtained from a water treatment plant in Mashhad. The main chemical constituents of DWTS are Fe_2O_3 (33.3%), SiO_2 (20.4%), CaO (8.1%), and Al_2O_3 (6.1%). The high quantity of iron in this sludge was associated with utilizing ferric chloride as a coagulant during the treatment of drinking water. More details about the properties of DWTS are reported in our previous work (Yazdani et al. 2019). Sodium hexametaphosphate ($(NaPO_3)_6, \geq 68\%$), sodium carbonate ($Na_2CO_3, \geq 99.9\%$), sodium chloride ($NaCl, \geq 99.5$), sodium hydroxide ($NaOH, \geq 99$–100%), potassium dichromate ($K_2Cr_2O_7, \geq 99.9\%$), lead nitrate ($Pb(NO_3)_2, \geq 99.5\%$), and hydrochloric acid (HCl, 37%) were acquired from Merck. Ethylenediamine ($C_2H_8N_2$, 99%) and ammonia (NH_3, 25%) were purchased from Sigma-Aldrich.

Clay extraction from bentonite

For clay extraction, first, 100 g of bentonite sample was sieved by 325 mesh and placed into a muffle furnace at 350°C to remove the organic matter. Second, 100 ml of HCl (12 M) was added to 50 g of the obtained sample and then washed with deionized water to eliminate carbonates (Bergaya and Lagaly 2013). Third, to remove the associated quartz, cristobalite, and other impurities (Gong et al. 2016; Klute and Page 1986; Sedighi et al. 2013), it dispersed in 2.5 L of distilled water, which containing and 0.9 g of sodium hexametaphosphate and 0.2 g of sodium carbonate, and centrifuged at 4000 rpm for 15 min. Finally, the above liquid was collected and dried at 70 °C for 24 h.

Nanoclay extraction

The nanoclay was separated from the clay fraction of bentonite using a method described by Calabi-Floody (Calabi-Floody et al. 2011). Five g of extracted clay is suspended in 300 ml of NaCl (1 M) and subjected to 50 watts of ultrasound for 5 min. The obtained mixture was centrifuged at 8000 rpm for 43 min. For removing mineral impurities, the preliminary round supernatant was discarded. After that, the precipitate was stirred with 50 ml of distilled water for 40 min and centrifuged again. The precipitate is agitated with 50 ml of distilled water for 40 min and then centrifuged. After collecting the upper portion of slurry, the solid was re-suspended in distilled water and centrifuged again. This stage was repeated 11 times. Finally, the attained supernatants were oven-dried at 70 °C and stored for the experiments. The extraction efficiency of nanoclay from bentonite was 40%.

Iron recovery

The collected sludge from the wastewater treatment plant was grounded and sieved. The resulting powder was then placed at 550° C for two h. Iron recovery was conducted according to the procedure described by Meng et al. (2016b). Twenty g of the obtained powder was mixed with 400 mL of hydrochloric acid and agitated at ambient temperature for 3 h. Then the mixture was passed through a filter paper to obtain the yellow liquid. The concentration of total Fe in the filtrate was 8723 mg/L, which was measured by an ICP-OES analyzer.

Synthesis of NC–Fe

The synthesis of green nano Fe supported on NC was done based on the modified method, which was demonstrated by Zhang et al. (2020). First, 1 g of NC was added to 60 ml of the solution obtained from acid-washed DWTS and stirred for 30 min. At the same time, a lemon Beebrush extract was made by adding 5 g of its powdered leaves to 400 mL of distilled water at 80 °C for 30 min. The obtained mixture was filtered twice through the filter paper after cooling to ambient temperature. Then, the extract was poured drop-wise into the NC and DWTS and mixed under a magnetic stirrer for 24 h. The mixture color was altered immediately to black, which indicated the nano Fe formation. After that, the suspension was centrifuged at 10000 rpm for 30 min. Finally, the obtained solid was washed with ethanol and dried at 80 °C.

The mechanism involved in the synthesis of iron nanoparticles can be explained as follows: lemon beebrush extract contains a variety of antioxidants and secondary metabolites, including verbascoside (Bilia et al. 2008; Cruz et al. 2010; Quirantes-Piné et al. 2009), chrysoeriol-7-O-diglucoronide (Cruz et al. 2010; Quirantes-Piné et al. 2009), isoverbascoside (Cruz et al. 2010; Quirantes-Piné et al. 2009), and luteolin-7-O-diglucoronide (Cruz et al. 2010; Quirantes-Piné et al. 2009), wherein these compounds act as reducing agent to reduce the Fe ions to the zero-valent iron nanoparticle and control its stability (Cruz et al. 2010; Mondal et al. 2020).

Synthesis of NC–Fe–N

The magnetic nanoclay composite (NCF) was functionalized via grafting using ethylenediamine, according to the method described by Ma et al. (2012). First, 0.4 g of NCF was mixed with 400 ml of distilled water and stirred for 24 h. Second, 9.0 mL ammonia and 4.8 mL ethylenediamine were added to the NCF suspension and stirred for 15 min. Third, the suspension was refluxed at 95 °C for 6 h. Forth, the obtained mixture was passed through a filter and washed with ethanol and distilled water. Ultimately, the resulting product was dried at 60 °C for 24 h and stored in a bottle for further experiments.

Characterization

The surface morphology of the NC and NCFN adsorbents was investigated using field emission scanning electron microscopy (FE-SEM) (TEACAN, MIRA lll, Czech Republic) technique. The thermogravimetric analysis (TGA) and derivative thermogravimetry (DTG) (Q600, TA, USA) were used to examine the thermal properties of clay materials with 20 °C/min at N_2. The functional groups on the surface of the adsorbent were determined by Fourier transform infrared spectroscopy (FTIR) (AVATAR, Thermo, USA) analysis.

Adsorption experiments

The batch mode adsorption tests were accomplished to evaluate the simultaneous removal of Cr(VI) and Pb(II) from aqueous solutions. To determine the optimum adsorption conditions, the effect of essential parameters such as pH (2–5), contact time (0–120 min), adsorbent dose (0.125–2.5 g/L), initial metal concentration (10–50 mg/L), and temperature (298–333 K) on the removal of abovementioned metal ions onto three adsorbent (DWTS, NC, and NCFN) was investigated. In each experiment, various amounts of adsorbents were added into an Erlenmeyer flask containing the 50 mL heavy metals ion solution with different concentrations, which was stirred at the desired temperature for a different time. For pH adjustment, the desired amount of dilute HCl or NaOH was used. After adsorption, the solution was filtered, and the residual concentration of Cr(VI) and Pb(II) was evaluated by atomic absorption spectrometry (AAS) (AA-7000, Shimadzu, Japan). The removal percentage ($R\%$) of metal ion was estimated using Eq. (S1). The adsorption capacity of adsorbent at time t was estimated using Eq. (S2).

Isothermal models

Langmuir adsorption model presumes uniform monolayer adsorption by the fixed number of the binding sites on the surface of the adsorbent. The nonlinearized Langmuir adsorption isotherm and its separation factor (R_L) are represented in Eq. (S3 and S4). The amount of R_L specifies the feasibility of the adsorption process. For $R_L > 1$, the adsorption is unfavorable, for $R_L = 1$, the adsorption is linear, for for $0 < R_L < 1$, the adsorption is favorable, and for $R_L = 0$, the adsorption is irreversible. The Freundlich model is an experiential adsorption isotherm equation, which assumes adsorption on diverse external sites and heat. Its equation model was described in Eq. (S5).

Adsorption kinetics

To evaluate the adsorption kinetics of Cr(VI) and Pb(II) ions, the pseudo-first-order and pseudo-second-order kinetic models were utilized. The pseudo-first-order (Eq. S7) presume that one adsorbate molecule adsorbed on one surface-active site of adsorbent while the pseudo-second-order (Eq. S8) assumes that one adsorbate molecule adsorbed on two active surface sites of adsorbent (Oskui et al. 2019; Subbaiah and Kim 2016). The initial adsorption rate (h) estimates from the pseudo-second-order kinetic model (Eq. S8).

Thermodynamic

Thermodynamic aid in recognizing the physical or chemical property of the adsorption mechanism. The thermodynamic factors such as Gibbs free energy change (ΔG), enthalpy change (ΔH), and entropy change (ΔS) were estimated from the equations (Eq. S8 and S9) (Van't Hoff) (Liu et al. 2017b). The slope and intercept of the linear plot of ln (Q_e/C_e) versus 1000/T were applied to estimate the quantities of ΔH and ΔS, respectively.

Results and discussion

Characterization of adsorbents

The morphology and the surface of the as-synthesized NC and NCFN adsorbents were evaluated by FE-SEM images (Fig. 1). As shown in Fig. 1a, the NC has a sheet structure, and no possible aggregation is observed. The configuration of NCFN in Fig. 1b presented that the spherical shape of Fe nanoparticles was dispersed on the surface of NC sheets. The size of Fe nanoparticle loaded on NC was ranged from 13 to 18 nm.

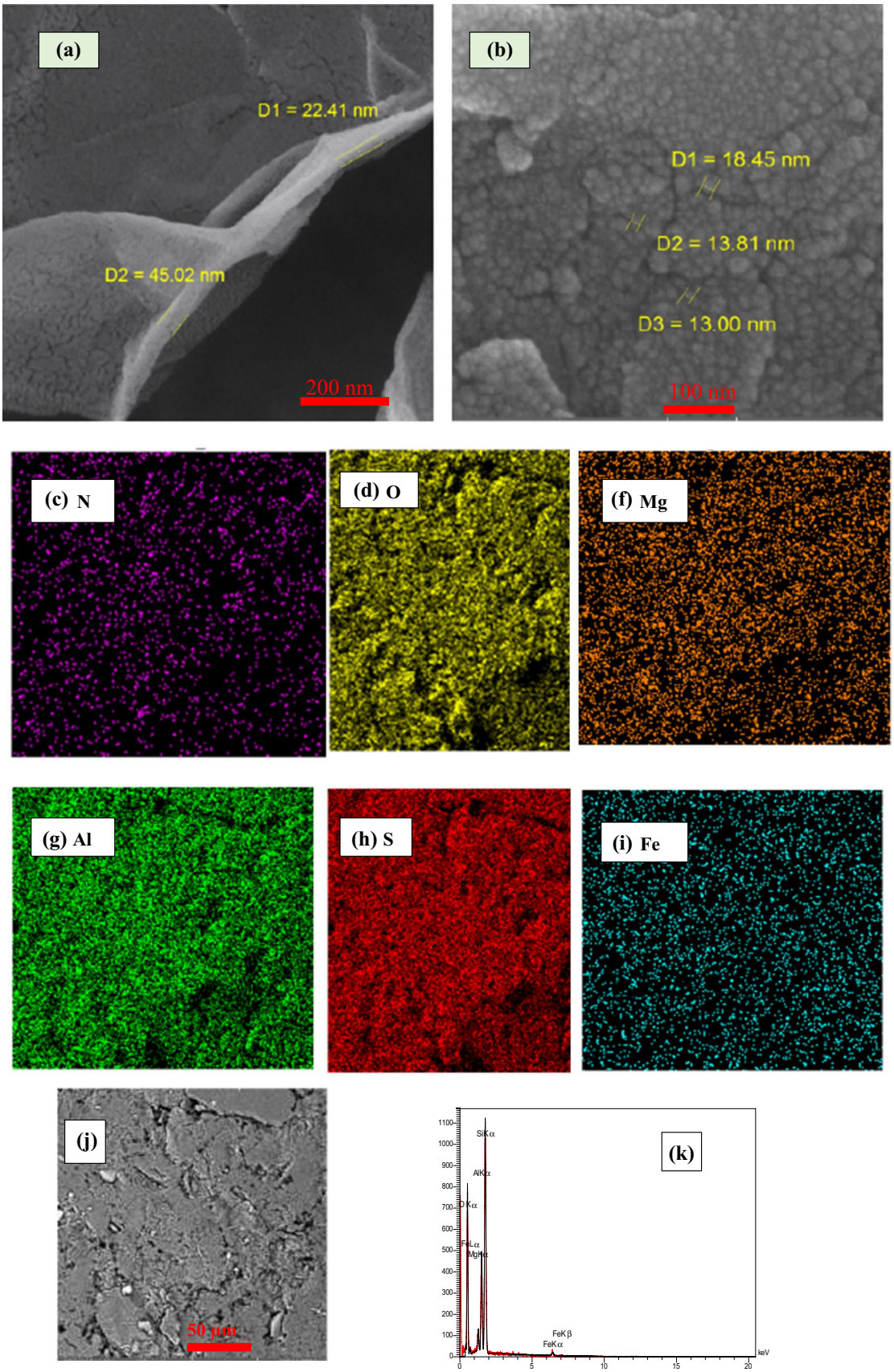

Fig. 1 The SEM image of NC and NCFN (**a**, **b**), and EDX mapping analysis of NCFN (**c**–**i**), its original SEM image (**j**), and corresponding elemental graph (**k**)

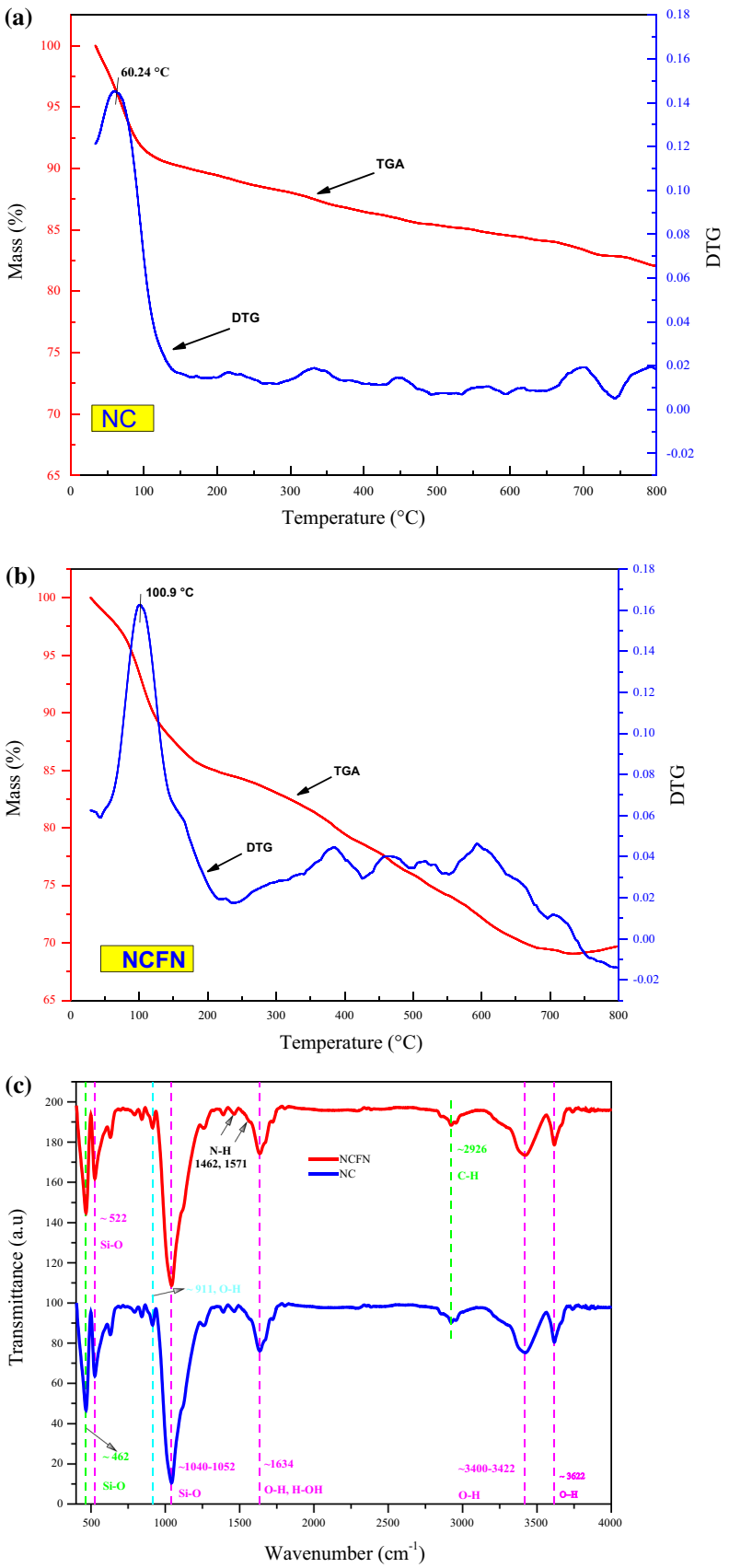

Fig. 2 The TGA and DTG curves, and FTIR spectra of NC (**a**) and NCFN (**b**)

Figure 1 presents the results of the energy-dispersive x-ray spectroscopy (EDX) analyses of NCFN. From its figure, the presence of Al, O, Si, Mg, N, and Fe atoms in the nanocomposite can be perceived. The elements are distributed uniformly on the surface. Al, Si, Mg, and O came mainly from the NC and the iron from the Fe nanoparticle synthesized from DWTS. N created mainly from the amine functional groups grafted ethylenediamine, which confirmed that the NCF had been successfully modified with ethylenediamine.

Figure 2 exhibits the TGA-DTG curves of NC and NCFN. The TGA curves display weight losses of 18 and 30.28% for NC and NCFN, respectively, over a temperature range between 30 and 800 °C. NC and NCFN had one step of mass loss at 60.24 and 100.9 °C, which ascribed to the removal of water molecules and free solvent in pores or interlayer of nanoclay (Celestino et al. 2019; Guggenheim and van Groos 2001; Li et al. 2019). The samples' backbone was thermally decomposed slowly. The significant weight loss of NC corresponded to the dehydroxylation of aluminosilicate groups in the clay structure (Li et al. 2019). The 12.28% higher loss of mass observed in the TGA curve of NCFN was related to (1) the pyrolysis of amine functional groups chemically grafted on its surfaces, (2) removal of physically adsorbed silanes, (3) the elimination of intercalated silanes, and (3) dehydroxylation of aluminosilicate groups (Asgari et al. 2017; Shanmugharaj et al. 2006; Wamba et al. 2017).

Figure 2 presents the FTIR spectra of NC and NCFN, which have similar peaks. The bands at 3622 and 3627 cm^{-1} were attributed to inner –OH stretching vibration in the octahedral structure of clay (Suraj et al. 1997). The broad bands observed at 3407 and 1639 cm^{-1} for NC, 3424, and 1634 cm^{-1} for NCFN were stretching and bending vibration of O–H and H–OH stretch vibrations of physisorbed water or the water molecules intercalated in the clay mineral (Bertuoli et al. 2014; Fayazi and Ghanbarian 2020; Li et al. 2019). Also, the bands at 1462 and 1571 cm^{-1} were related to the bending vibrations of the amine ($–NH_2$) (Asgari et al. 2017; Bertuoli et al. 2014; Hu et al. 2017). These peaks show the grafting of ethylenediamine molecules on the tetrahedral sheets of nanoclay. The peaks located at 2926 cm-1 are recognized to the C-H asymmetric aliphatic groups (Chen et al. 2017; Moreira et al. 2017). The presence of the sharp peak at 1040 and 1052 cm^{-1} were connected to the Si–O stretching vibration (Luo et al. 2017). Bending vibration of Si–O–Al, and Si–O–Si was observed at 462 cm^{-1} (Suraj et al. 1997). Two bands located at 791 and 794 cm^{-1} were assigned to Si–O vibration of quartz impurities (Bekri-Abbes and Srasra 2016). Other peaks were noticed at 911 cm^{-1} are attributed to the bending vibration of –OH in Al–OH (Li et al. 2019; Tyagi et al. 2006). The strong peaks were observed at 462 and 522 cm^{-1} are related to vibration of Si–O–Si (Suraj et al. 1997; Tyagi et al. 2006). However, based on the presence of the critical functional groups such as $–NH_2$ and –OH involved in the adsorption of heavy metal, it is expected that the NC and NCFN to be appropriate adsorbents.

Adsorption study

Effect of adsorbent dose

Figure 3 presents the influence of adsorbent quantity on the Cr(VI) and Pb(II) removal onto DWTS, NC, and NCFN. As the three adsorbent doses improved from 0.125 to 2.5 g/L, the removal performance of Cr(VI) and Pb(II) enhanced and leaned toward to reach steady at the greater quantity. The removal percentage of Cr(VI) enhanced from 38.69 to 62.36% (for DWTS), from 47.37 to 74.02% (NC), and from 56.22 to 84.70% (NCFN). That of Pb(II) raised from 33.47 to 46.63% (for DWTS), from 34.13 to 53.19% (for NC), and from 30.05 to 60.50% (for NCFN). This phenomenon occurs because of the rise in the number of active reaction places for the uptake of metal ions (Liu et al. 2017a; Naseem and Tahir 2001). Besides, the adsorption capacity of three adsorbents diminished with an increment of adsorbent mass. This decreasing trend may be ascribed to (1) the growth of the number of the unsaturated adsorption sites on the adsorbent at a higher dosage and (2) aggregation of adsorbent at higher mass, causing a reduction in its total surface area and as a result, adsorption (Sharma et al. 2014). The NCFN had the greatest adsorption amounts for both metal ions rather than DWTS and NC due to the modification of nanoclay by iron and amine. The adsorption capacity of NCFN for Cr(VI) and Pb(II) was 1.72 and 0.145 mmol/g, respectively. An adsorbent quantity of 0.5 g/L was taken as the optimal dosage for consequent adsorption experiments.

Effect of initial pH

The pH of the metal solution is critical factor that has a significant influence on the adsorption capacity of an absorbing substance and the removal performance of adsorbate (heavy metals ions). Figure 4 displays the influence of pH on removing Cr(VI) and Pb(II) ions for all adsorbents. From Fig. 4, the removal of Cr(VI) from aqueous solution enhanced with decreasing pH value from 5 to 2 in agreement with previous researches (Yuan et al. 2010; Zhang et al. 2018). The maximum Cr(VI) removal efficiency reached 53.2, 62.5, and 84.4% for DWTS, NC, and NCFN, respectively, when the initial pH was 3. It implied that in pH 3 high extent protonation of adsorbent surface groups (e.g., –OH and $–NH_2$, Fe) was happened, which generates powerful, attractive forces between these positive charges of adsorption sites and the negative charges of Cr(VI) species ($HCrO_4^-$ and $Cr_2O_7^{2-}$)

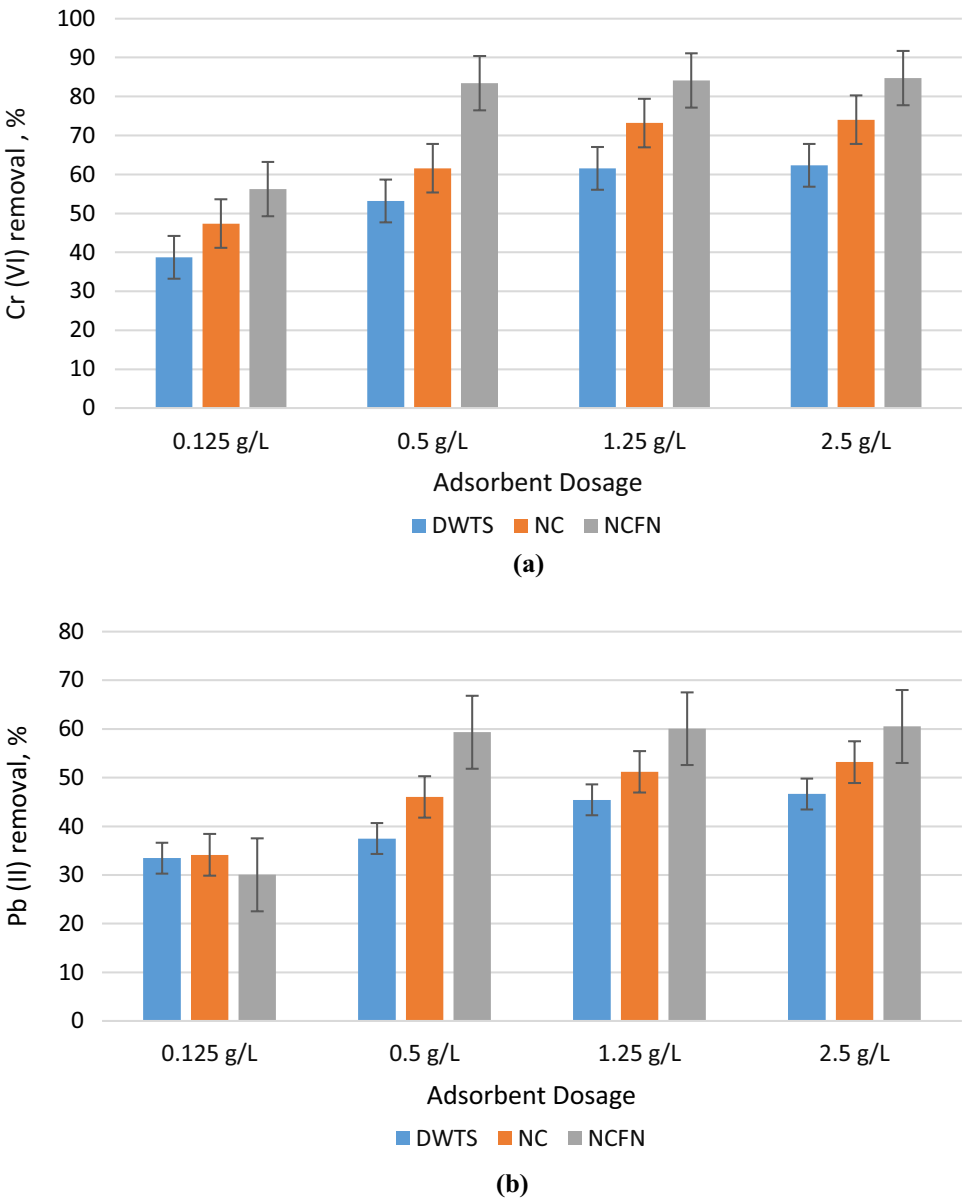

Fig. 3 The influence of adsorbent dose of DWTS, NC, and NCFN on Cr(VI) and Pb(II) removal. Experimental conditions: adsorbent dosage: (0.125–2.5 g/L); initial metal concentration: 20 mg/L; pH: 3; temperature: 25°C; and contact time: 60 min

(Jain et al. 2018; Saha and Orvig 2010; Yadav et al. 2013). In contrast, the reduction in the removal efficiency at pH higher than 3 happened because the surface of adsorbents would be hindered due to electrostatic repulsion. In other words, under acidic conditions, corrosion of Fe present in DWTS and NCFN adsorbents increased, which created more reactive sites and supporting the reduction reactions (Zhu et al. 2018a).

The removal efficiency of Pb(II) ion enhanced with an increment of pH from 2 to 5 (Fig. 4b), which was inconsistent with prior researches (Forghani et al. 2020; Fu et al. 2015; Kumari et al. 2015). The highest removal efficiency of Pb(II) at pH of 5 was 73.55, 52.745, and 50.36% for NCFN, NC, and DWTS, respectively. This phenomenon happened due to the high production of hydronium ions (H_3O^+) in the solution at lower pH, which leads to competition between Pb^{2+} ions for adsorption onto adsorbents, thereby dropping the adsorption efficiency of this ion (Li et al. 2019). These findings are in agreement with Li et al. (Li et al. 2019) results, which evaluated the adsorption of Pb(II) cations and Cr(VI) anions from aqueous solution using amino-modified nano-sized illite–smectite clay. They found that

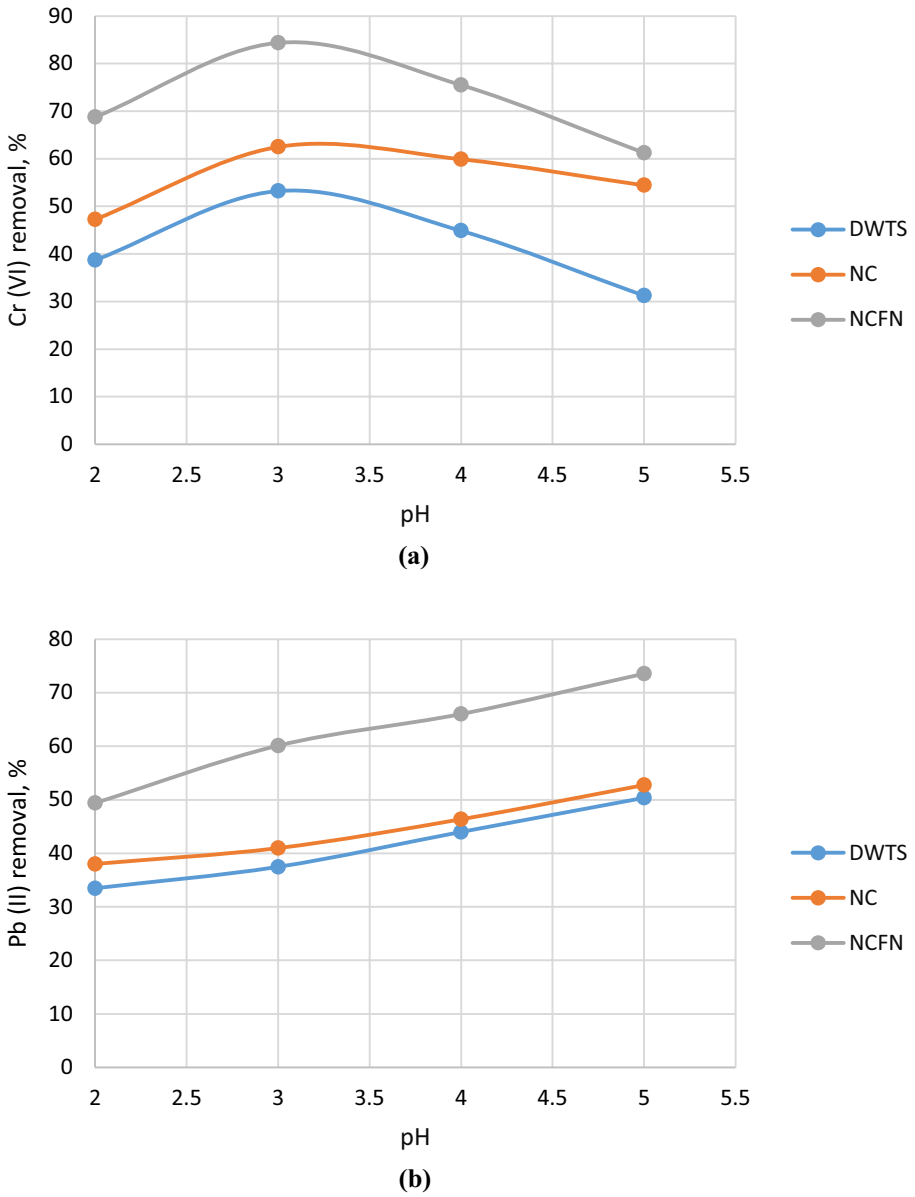

Fig. 4 The influence of pH on Cr(VI) and Pb(II) removal by DWTS, NC, and NCFN. Experimental conditions: pH (2–5), initial metal concentration: 20 mg/L; adsorbent dosage: 0.5 g/L; temperature: 25 °C; and contact time: 60 min

the maximum Cr(VI) and Pb(II) removals were obtained at a pH of 2.2 and 5.5, respectively. The adsorption efficiency was highest at pH 3 for Cr(VI) using NCFN adsorbent. Due to the better adsorption performance of all adsorbents for Cr(VI) than Pb(II), its optimal pH (3) was used in the next experiments.

Isothermal models

The simultaneous adsorption of binary metal ions (Cr(VI) and Pb(II)) on the adsorbents was analyzed using Freundlich and Langmuir isotherms, and their plots are presented in Fig. 5. The adsorption data of both ions (Cr(VI) and Pb(II)) by three adsorbents (DWTS, NC, and NCFN) were fitted better with the Langmuir ($R^2 > 0.97$) than Freundlich model ($R^2 > 0.93$). The fit of equilibrium data by the Langmuir indicated that the adsorption of metal ions happens on the monolayer of DWTS, NC, and NCFN. Table 1 lists the calculated parameter from the abovementioned isotherm models. As shown in this table, the separation factors (R_L) calculated from Langmuir isotherms were between 0 and 1; as a consequence of that, the Pb(II) and Cr(VI) ions removal by all adsorbents is favorable. Besides, the estimated n (Freundlich

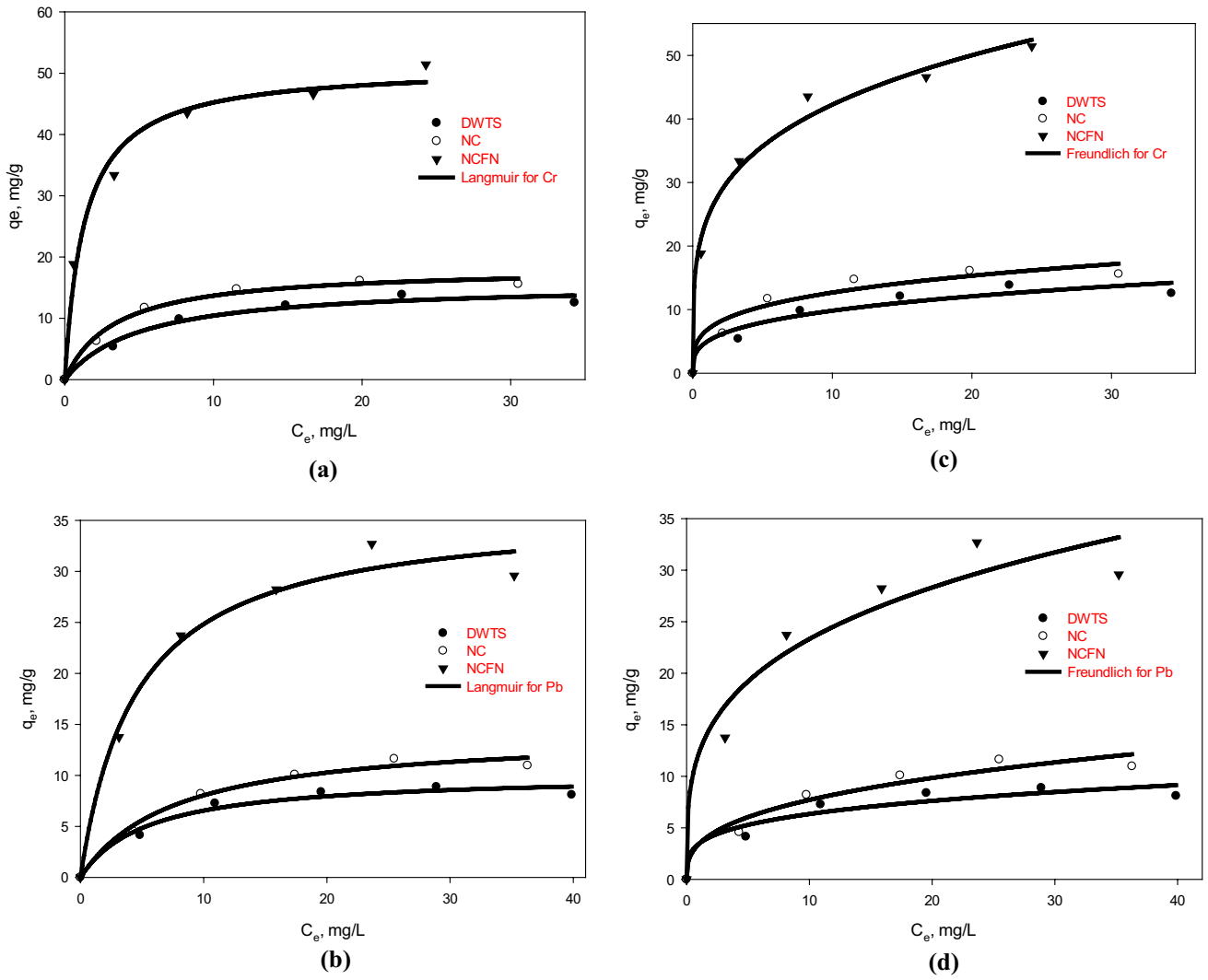

Fig. 5 The adsorption isotherms of Cr(VI) and Pb(II) on DWTS, NC, and NCFN adsorbents. **a**, **b** Langmuir model, **c**, **d** Freundlich model. Experimental conditions: initial metal concentration: (10–50 mg/L); pH 3; adsorbent dosage: 0.5 g/L; temperature: 25 °C; and contact time: 60 min

constant) was more significant than 1, which confirms a favorable circumstance for metal ion adsorption.

The maximum adsorption quantity (q_m) of Cr(VI) estimated by the Langmuir isotherm model for DWTS, NC, and NCFN was 0.303, 0.352, and 0.984 mmol/g, respectively. The amount of q_m for Pb(II) by DWTS, NC, and NCFN was 0.03, 0.042, and 0.108 mmol/g, respectively. This finding was compared with the maximum adsorption capacity of different clay adsorbents (Table 2). From Table 2, the raw clay had a relatively low q_m for metal ions. For instance, the q_m of clay for Cr(VI) and Pb(II) removal was obtained as 0.01 and 0.066 mmol/g, respectively (Khan and Singh 2010). However, the modification of clay adsorbents with metals (e.g., Fe) and amine materials enhanced their adsorption capacity for metal ions. For example, the q_m quantity of raw kaolin for Pb(II) removal improved from 0.014 to 0.097 mmol/g after the modification by aluminum sulfate (Jiang et al. 2009). In this study, after modification of nanoclay with iron and amine groups, the q_m of Cr(VI) ion improved from 0.352 to 0.984 mmol/g. A similar increment trend (from 0.042 to 0.108 mmol/g) was observed for Pb(II) ion in the binary system.

Surface complexation, ion exchange, and surface precipitation were the processes involved in heavy metals removal by clay adsorbent (Gahlot et al. 2020; Shi et al. 2011; Yuan et al. 2013). Surface complexation happens by

Table 1 Isotherm and kinetic parameters for the removal of Cr(VI) and Pb(II) by DWTS, NC, and NCFN

Adsorbent	Metals	Langmuir isotherm model				Freundlich isotherm model			Pseudo-first-order			$q_{e,exp}$ (mg/g)	Pseudo-second-order			h (mg/(g min))
		q_m (mg/g)	b (L/mg)	R^2	R_L	K_f (mg/g)	n (L/mg)	R^2	K_1 (1/min)	q_{e1} (mg/g)	R^2		K_2 (g/(mg min))	q_{e2} (mg/g)	R^2	
DWTS	Cr(VI)	15.7732	0.1956	0.9778	0.34–1	4.9274	3.3373	0.9382	0.0612	28.50	0.9732	21.92	0.0022	25.51	0.9926	1.0578
	Pb(II)	10.1276	0.1830	0.9721	0.40–1	3.4546	3.7917	0.9361	0.0400	19.16	0.9928	16.41	0.0015	21.00	0.9909	0.4043
NC	Cr(VI)	18.3348	0.2952	0.9891	0.25–1	6.7512	3.6559	0.9471	0.0860	22.37	0.8541	25.17	0.007	26.52	0.9954	4.4356
	Pb(II)	14.2192	0.1302	0.9857	0.97–1	3.4266	2.8406	0.9573	0.080	27.13	0.9877	18.73	0.0042	20.83	0.9963	1.4747
NCFN	Cr(VI)	51.2050	0.7568	0.9848	0.12–1	24.1242	4.1100	0.9896	0.0810	7.83	0.7568	34.04	0.0692	34.13	1.0000	80.2080
	Pb(II)	36.0650	0.2212	0.9833	0.97–1	12.2404	3.5703	0.9511	0.0785	14.78	0.7787	24.40	0.0063	25.97	0.9954	3.7531

forming ionic and covalent bonds between heavy metals ions and surface OH groups and O atoms of the edges of the clay. The affinity and preference of adsorption sites of aluminosilicate structure for various adsorbates were determined by ionic strength, pH, and the presence of anions in the solution (Gahlot et al. 2020). With coating Fe nanoparticle on the surface of NC, removing heavy metals ions from aqueous solution increased due to reduction, absorption, and precipitation mechanism (Fu et al. 2015; Yang et al. 2019). Cr(VI) and some of Pb(II) in the solution adsorbed onto the surface of the NCFN and then reduced to Cr(III) and Pb^0 by Fe (Zhang et al. 2011). Cr(III) was eliminated from the aqueous solution by precipitation (in the form of $Cr(OH)_3$ or $Fe_{(1-x)}Cr_x(OH)_3$ (Toli et al. 2016). The Pb^0 and a hydroxylated $Cr(OH)_3$ species precipitated on the NCFN (Shi et al. 2011; Zhang et al. 2011). Introducing amine groups into the NC-Fe enhanced the heavy metals removal because these functional groups can act as the Lewis base for bonding with cations. The Pb(II) and Cr(III) cations in the solution were electrostatically attracted by protonated amine groups by the surface complexation mechanism (Fayazi and Ghanbarian 2020). A similar mechanism for Cr(VI) and Pb(II) uptake by nanoclay functionalized adsorbent by iron and amine was reported in previous studies (Fayazi and Ghanbarian 2020; Fu et al. 2015).

Effect of contact time and adsorption kinetics

Figure 6 shows the effect of contact time on the removal efficiency of Cr(VI) and Pb(II) by DWTS, NC, and NCFN adsorbents. It can be seen that the removal efficiencies of both metal ions onto three abovementioned adsorbents were raised rapidly until 30 min and then reach a plateau after 120 min. The high rates of Cr(VI) and Pb(II) removal at the beginning of adsorption were attributed to the high accessibility of the unoccupied adsorption site, which is located in the exterior of the adsorbent. For DWTS and NC adsorbents, the adsorption equilibrium was acquired at 60 min, while for NCFN, it achieved at 30 min. The obtained equilibrium time was similar to that reported for montmorillonite-supported magnetite nanoparticles (Yuan et al. 2009) and bentonite-supported nanoscale zero-valent iron (Shi et al. 2011) for Cr(VI).

The kinetic data of the metal mentioned above were proportionated to the pseudo-first- and pseudo-second-order models (Fig. 6 and Table 1). the R^2 values were obtained for the second-order kinetic model were higher than those acquired for the first-order. Besides, as shown in Table 1, the $q_{e,exp}$, and the q_{e1} and q_{e2} (calculated q_e) quantities for the second-order model were approximately near to each other. Therefore, from the finding, it could be understood that the adsorption of Cr(VI) and Pb(II) ion

Table 2 Comparison of maximum adsorption capacity of clay materials for Cr(VI) and Pb(II) ions

Adsorbents	Adsorption capacity (mmol/g)		Condition	References
	Pb(II)	Cr(VI)		
MMT-Fe_3O_4-PEI nanocomposite	–	1.209	Single system	Fayazi and Ghanbarian (2020)
MMT- magnetite nanoparticles	–	0.294	Single system	Yuan et al. (2009)
B-nZVI	–	0.359	Single system	Shi et al. (2011)
Clay	0.01	0.066	Single system	Khan and Singh (2010)
Mag	–	0.387	Single system	Yuan et al. (2009)
MMT- Mag	–	0.266		
Raw kaolin	0.014	–	Single system	Jiang et al. (2009)
Modified kaolin	0.097	–		
NH_2-NI/S	0.336	0.612	Binary system	Li et al. (2019)
S-NZVI	0.133	0.843	Binary system	Fu et al. (2015)
FA-ZVI	0.235	0.301	Binary system	Liu et al. (2017a)
DWTS	0.03	0.303	Binary system	This work
NC	0.042	0.352		
NCFN	0.108	0.984		

MMT montmorillonite, *PEI* polyethyleneimine, *SAC* spent activated clay, *NI/S* nano illite–smectite, *Mag* magnetite nanoparticles, *S-NZVI* sepiolite-nano zero-valent iron, *B-nZVI* Bentonite-nano zero-valent iron, *FA-ZVI* fly ash- zero-valent iron

onto DWTS, NC, and NCFN pursued the pseudo-second-order kinetic model. In other words, it indicated that the adsorption phenomenon happened through a covalent bond (e.g., sharing of electrons and electron exchange) between adsorbent and adsorbate (Ho and McKay 1999). Analogous findings were reported for the kinetic adsorption of the aftermentioned ions on different adsorbents (Alghamdi et al. 2020). Also, for both ions, the most significant h was obtained for NCFN, implying that adsorbent modification improved the adsorption rate (Fig. 6).

Thermodynamic Studies

Figure 7 presents the Van't Hoff graphs for adsorption of metal ions onto DWTS, NC, and NCFN. The related parameters were summarized in Table 3. For Pb(II) ion, the values of ΔG° was minus at entire temperatures, implying that its adsorption system is thermodynamically extemporaneous in nature. Besides, ΔG° values for DWTS and NC adsorbents were lesser than − 20 kJ/mol, demonstrating that the adsorption process was physical. At the same time, that of NCFN was higher than − 20 kJ/mol, showing the process was chemical adsorption (Horsfall Jr et al. 2006). Moreover, for Pb(II), the negative quantities of ΔH°, and the positive amounts of ΔS indicate that its reaction was exothermic. Interface between solid and solution enhanced randomly, respectively. The exothermic adsorption of Pb(II) was reported by other clay materials (Yadava et al. 1991).

For Cr(VI) ion, at all temperatures, the amounts of ΔG° were positive, presenting a spontaneous adsorption process, and consequently, some energy from an external source needs to happen. Furthermore, the positive quantities of ΔH° suggested that as the endothermic process. At the same time, the negative values of ΔS show that the degrees of freedom were lost with the formation of the activated complex (León-Torres et al. 2012). Endothermic adsorption of Cr(VI) onto clay adsorbents was confirmed by other researchers (Bhattacharyya and Sen Gupta 2006; Khan and Khan 1995).

Removal Cr(VI) and Pb(II) from real wastewater

The possibility/capability of three adsorbents (DWTS, NC, and NCFN) for removal of Cr(VI) and Pb(II) ions from industrial wastewater was investigated. Two wastewater samples (1 and 2) were collected from a tannery plant in northeast Iran. In a typical experiment, 25 mL of wastewater was added to 0.01 g of the adsorbents in 25 mL under constant stirring at a pH of 3 for 60 min. In sample 1, the Cr(VI) and Pb(II) in the wastewater were low, 2, and 0.5 mg/L. The results indicated that both metal ions were removed entirely from industrial effluent on DWTS, NC, and NCFN. Moreover, the initial concentrations of Cr(VI) and Pb(II) were 19

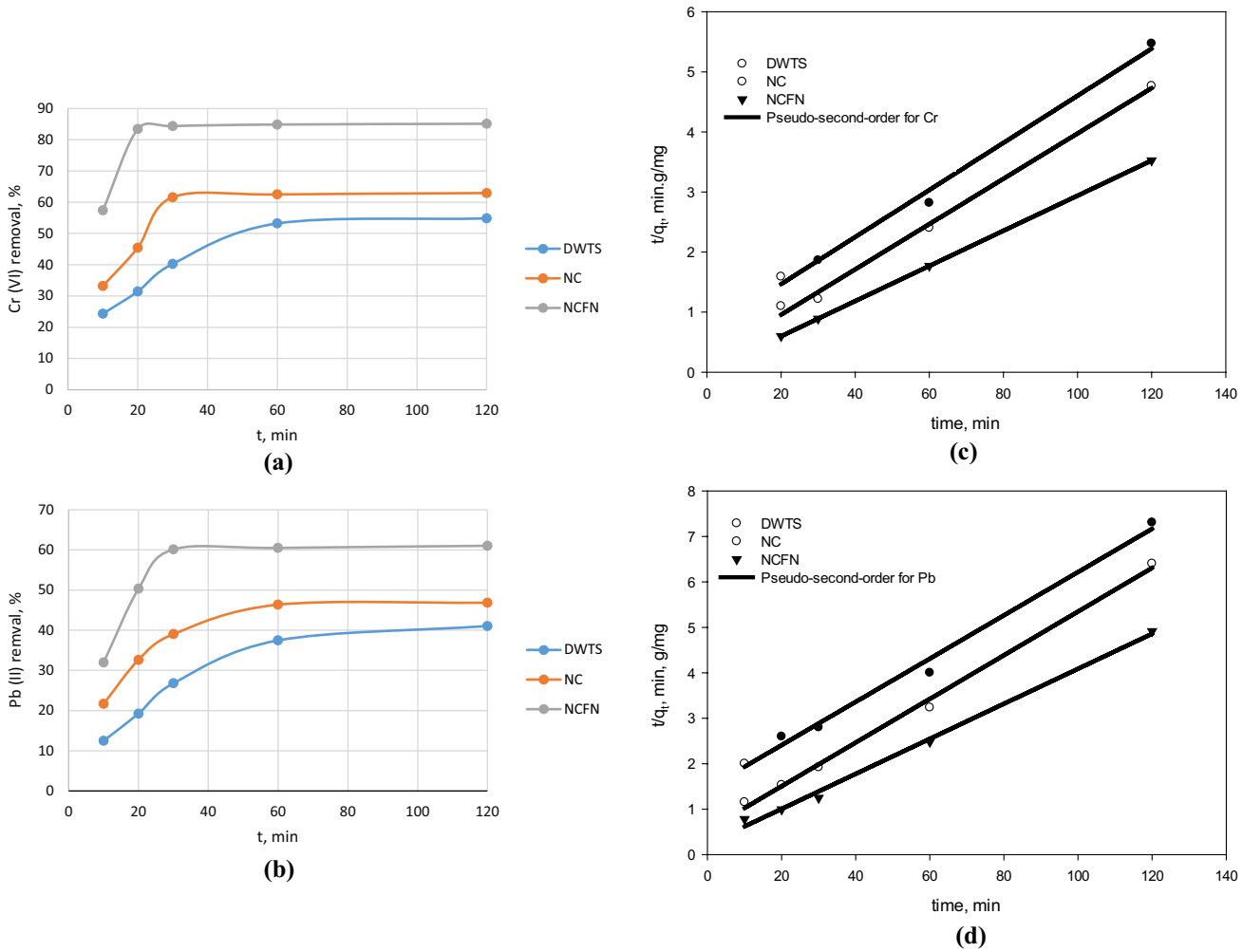

Fig. 6 Contact time (**a**, **b**) and the pseudo-second-order kinetics (C and d) of Cr(VI) and Pb(II) adsorption onto DWTS, NC, and NCFN. Experimental conditions: contact time: (0–120 min); initial metal concentration: 20 mg/L; pH: 3; adsorbent dosage: 0.5 g/L; and temperature: 25 °C

and 9 mg/L, in sample 2. The removal efficiency of Cr(VI) was 80, 69, and 58% for NCFN, NC, and DWTS, respectively. In the case of Pb(II), the removal percentage was 60, 52, and 48% for NCFN, NC, and DWTS, respectively.

Conclusion

DWTS is an iron-rich waste, which is used as an adsorbent and also a raw material for the synthesis of the new adsorbent. Nanoscale Fe nanoparticle-supported nanoclay was successfully green synthesized from DWTS as a source of iron and lemon beebrush extract as a reducing agent. To improve the adsorption ability of nanoclay containing Fe (NCF), it is grafted with ethylenediamine. The SEM, EDX, FTIR, and TGA analyses confirmed that the iron nanoparticle and amine functional groups were immobilized on nanoclay. The ability of adsorption of Cr(VI) and Pb(II) onto DWTS, NC, and NCFN was compared. The results showed that the removal of Cr(VI) and Pb(II) enhanced with an increment of contact time and adsorbent dosage. The Langmuir isotherm model indicated the best fit to equilibrium empirical data of two metals. The q_m of Cr(VI) onto DWTS, NC, NCFN was 0.303, 0.352, and 0.984 mmol/g, while the values of Pb(II) were 0.03, 0.042, and 0.108 mmol/g,

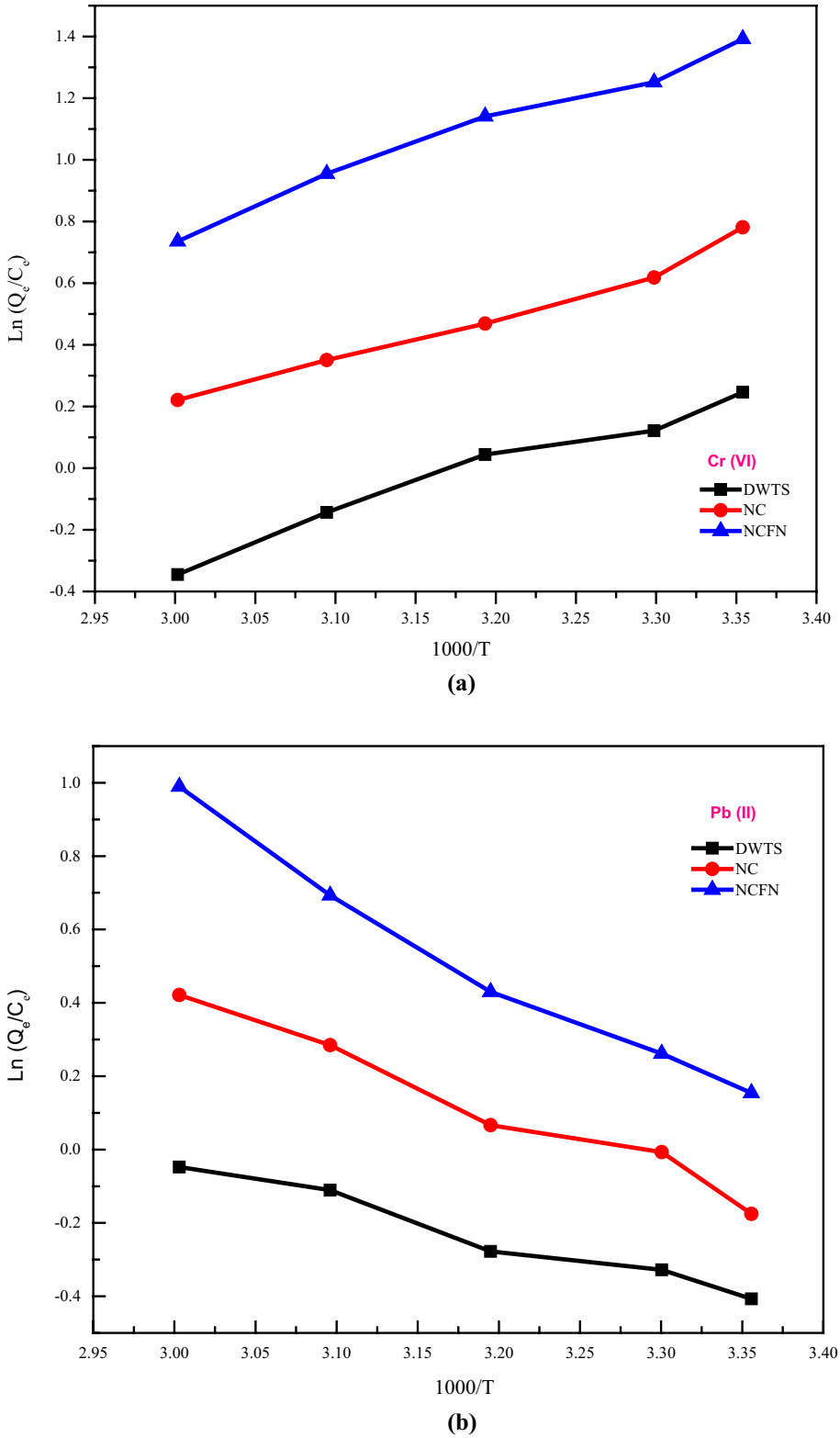

Fig. 7 Van't Hoff plots for adsorption of Cr(VI) and Pb(II) onto DWTS, NC, and NCFN. Experimental conditions: initial metal concentration: (10–50 mg/L); pH 3; adsorbent dosage: 0.5 g/L; temperature: 25 °C; and contact time: 60 min

respectively. For both metal ions, the q_m of NCFN was superior to that of DWTS and NC. The removal percentage of Pb(II) and Cr(VI) enhanced with increasing contact time and adsorbent dose. The kinetic data of Cr(VI) and Pb(II)

Table 3 Thermodynamic factors for adsorption of Cr(VI) and Pb(II) by DWTS, NC, and NCFN

Metal	Adsorbent	Temperature (K)	ΔG (kJ/mol)	ΔH (kJ/mol)	ΔS J/(K mol))
Cr(VI)	DWTS	298	1513.93	1.586	− 5.075
		303	1539.31		
		313	1590.06		
		323	1640.81		
		333	1691.56		
	NC	298	1287.37	1.505	− 4.315
		303	1308.95		
		313	1352.1		
		323	1395.25		
		333	1438.4		
	NCFN	298	1351.405	1.763	− 4.529
		303	1374.05		
		313	1419.34		
		323	1464.63		
		333	1509.92		
Pb(II)	DWTS	298	− 907.06	− 1.026	3.0404
		303	− 922.26		
		313	− 952.67		
		323	− 983.07		
		333	− 1013.48		
	NC	298	− 1575.09	− 1.6183	5.2801
		303	− 1601.49		
		313	− 1654.29		
		323	− 1707.09		
		333	− 1759.89		
	NCFN	298	− 2358.61	− 2.3202	7.907
		303	− 2398.14		
		313	− 2477.21		
		323	− 2556.28		
		333	− 2635.35		

was fitted well with the pseudo-second-order model. Thermodynamic data showed that the adsorption process of Pb(II) was exothermic and spontaneous, as that of Cr(VI) was endothermic and non-spontaneous. It can be concluded that the NCFN could be utilized as an effective adsorbent for the elimination of Cr(VI) and Pb(II) metal from aqueous solution.

Acknowledgements We would like to thank the Ferdowsi University of Mashhad (FUM) for funding this project (Research ID 45180). We also hearty appreciated the guidance of Dr. Alireza Karimi who helped us with the purification of bentonite in the laboratory.

References

Abbassi R, Yadav AK, Kumar N, Huang S, Jaffe PR (2013) Modeling and optimization of dye removal using "green" clay supported iron nano-particles. Ecol Eng 61:366–370. https://doi.org/10.1016/j.ecoleng.2013.09.040

Ahmad T, Ahmad K, Alam M (2016) Sustainable management of water treatment sludge through 3'R' concept. J Clean Prod 124:1–13. https://doi.org/10.1016/j.jclepro.2016.02.073

Alghamdi AA, Al-Odayni AB, Saeed WS, Al-Kahtani A, Alharthi FA, Aouak T (2020) Efficient adsorption of lead (II) from aqueous phase solutions using polypyrrole-based activated carbon. Materials 12:1–16

Asgari M, Abouelmagd A, Sundararaj U (2017) Silane functionalization of sodium montmorillonite nanoclay and its effect on rheological and mechanical properties of HDPE/clay nanocomposites. Appl Clay Sci 146:439–448. https://doi.org/10.1016/j.clay.2017.06.035

Bekri-Abbes I, Srasra E (2016) Effect of mechanochemical treatment on structure and electrical properties of montmorillonite. J Alloy Compd 671:34–42. https://doi.org/10.1016/j.jallcom.2016.02.048

Bello A, Leiviskä T, Zhang R, Tanskanen J, Maziarz P, Matusik J, Bhatnagar A (2019) Synthesis of zerovalent iron from water treatment residue as a conjugate with kaolin and its application for vanadium removal. J Hazard Mater 374:372–381. https://doi.org/10.1016/j.jhazmat.2019.04.056

Bergaya F, Lagaly G (2013) Purification of natural clays. In: Faïza Bergaya BKG, Theng GL (eds) Developments in clay science, vol 5. Elsevier, UK, Netherland, pp 213–221

Bertuoli PT, Piazza D, Scienza LC, Zattera AJ (2014) Preparation and characterization of montmorillonite modified with 3-aminopropyltriethoxysilane. Appl Clay Sci 87:46–51. https://doi.org/10.1016/j.clay.2013.11.020

Bhattacharyya KG, Sen Gupta S (2006) Adsorption of chromium(VI) from water by clays. Ind Eng Chem Res 45:7232–7240

Bian R, Zhu J, Chen Y, Yu Y, Zhu S, Zhang L, Huo M (2019) Resource recovery of wastewater treatment sludge: synthesis of a magnetic cancrinite adsorbent RSC. Advances 9:36248–36255

Bilia A, Giomi M, Innocenti M, Gallori S, Vincieri F (2008) HPLC–DAD–ESI–MS analysis of the constituents of aqueous preparations of verbena and lemon verbena and evaluation of the antioxidant activity. J Pharm Biomed Anal 46:463–470

Bolisetty S, Peydayesh M, Mezzenga R (2019) Sustainable technologies for water purification from heavy metals: review and analysis. Chem Soc Rev 48:463–487. https://doi.org/10.1039/C8CS00493E

Calabi-Floody M, Bendall JS, Jara AA, Welland ME, Theng BKG, Rumpel C, Mora MDL (2011) Nanoclays from an Andisol: extraction, properties and carbon stabilization. Geoderma 161:159–167. https://doi.org/10.1016/j.geoderma.2010.12.013

Celestino GG, Henriques RR, Shiguihara AL, Constantino VRL, de Siqueira Melo R, Amim Júnior J (2019) Adsorption of gallic acid on nanoclay modified with poly(diallyldimethylammonium chloride). Environ Sci Pollut Res 26:28444–28454. https://doi.org/10.1007/s11356-018-3505-x

Chen W, Zhang X, Mamadiev M, Zhao C, Wang Z, Xu H (2017) Synthesis of interstratified graphene/montmorillonite composite material through organics-pillared, delamination and co-stacking and its application in hexavalent chromium removal from aqueous solution. Adv Powder Technol 28:521–533. https://doi.org/10.1016/j.apt.2016.10.021

Cruz D, Falé PL, Mourato A, Vaz PD, Serralheiro ML, Lino ARL (2010) Preparation and physicochemical characterization of Ag nanoparticles biosynthesized by *Lippia citriodora* (Lemon Verbena). Colloids Surf B 81:67–73

da Silva E, Morita D, Lima A, Teixeira LG (2015) Manufacturing ceramic bricks with polyaluminum chloride (PAC) sludge from a water treatment plant. Water Sci Technol 71:1638–1645

Evuti AM, Lawal M (2011) Recovery of coagulants from water works sludge: a review. Adv Appl Sci Res 2:410–417

Fayazi M, Ghanbarian M (2020) One-pot hydrothermal synthesis of polyethylenimine functionalized magnetic clay for efficient removal of noxious Cr(VI) from aqueous solutions. Silicon 12:125–134. https://doi.org/10.1007/s12633-019-00105-9

Foo KY, Hameed BH (2010) Insights into the modeling of adsorption isotherm systems. Chem Eng J 156:2–10. https://doi.org/10.1016/j.cej.2009.09.013

Forghani M, Azizi A, Livani MJ, Kafshgari LA (2020) Adsorption of lead(II) and chromium(VI) from aqueous environment onto metal-organic framework MIL-100(Fe): synthesis, kinetics, equilibrium and thermodynamics. J Solid State Chem 291:121636. https://doi.org/10.1016/j.jssc.2020.121636

Frías M, De La Villa RV, De Soto I, Garcia R, Baloa T (2014) Influence of activated drinking-water treatment waste on binary cement-based composite behavior: characterization and properties. Compos B Eng 60:14–20

Fu R, Yang Y, Xu Z, Zhang X, Guo X, Bi D (2015) The removal of chromium (VI) and lead (II) from groundwater using sepiolite-supported nanoscale zero-valent iron (S-NZVI). Chemosphere 138:726–734. https://doi.org/10.1016/j.chemosphere.2015.07.051

Gahlot R, Taki K, Kumar M (2020) Efficacy of nanoclays as the potential adsorbent for dyes and metal removal from the wastewater: a review. Environ Nanotechnol Monit Manag 14:100339. https://doi.org/10.1016/j.enmm.2020.100339

Gong Z, Liao L, Lv G, Wang X (2016) A simple method for physical purification of bentonite. Appl Clay Sci 119:294–300

Guggenheim S, van Groos AFK (2001) Baseline studies of the clay minerals society source clays: thermal analysis. Clays Clay Miner 49:433–443. https://doi.org/10.1346/ccmn.2001.0490509

Gupta VK, Gupta D, Agarwal S, Kothiyal NC, Asif M, Sood S, Pathania D (2016) Fabrication of chitosan-g-poly(acrylamide)/Cu nanocomposite for the removal of Pb(II) from aqueous solutions. J Mol Liq 224:1319–1325. https://doi.org/10.1016/j.molliq.2016.10.118

He C, Yang Z, Ding J, Chen Y, Tong X, Li Y (2017) Effective removal of Cr(VI) from aqueous solution by 3-aminopropyltriethoxysilane-functionalized graphene oxide. Colloids Surf A 520:448–458. https://doi.org/10.1016/j.colsurfa.2017.01.086

Ho YS, McKay G (1999) Pseudo-second order model for sorption processes. Process Biochem 34:451–465. https://doi.org/10.1016/S0032-9592(98)00112-5

Horsfall M Jr, Abia A, Spiff A (2006) Kinetic studies on the adsorption of Cd2+, Cu2+ and Zn2+ ions from aqueous solutions by cassava (Manihot sculenta Cranz) tuber bark waste. Biores Technol 97:283–291

Hu X et al (2017) Ethylenediamine grafted to graphene oxide@Fe_3O_4 for chromium(VI) decontamination: performance, modelling, and fractional factorial design. PLoS ONE 12:e0187166. https://doi.org/10.1371/journal.pone.0187166

Jain M, Yadav M, Kohout T, Lahtinen M, Garg VK, Sillanpää M (2018) Development of iron oxide/activated carbon nanoparticle composite for the removal of Cr(VI), Cu(II) and Cd(II) ions from aqueous solution. Water Resour Ind 20:54–74. https://doi.org/10.1016/j.wri.2018.10.001

Jiang M-Q, Wang Q-P, Jin X-Y, Chen Z-L (2009) Removal of Pb(II) from aqueous solution using modified and unmodified kaolinite clay. J Hazard Mater 170:332–339. https://doi.org/10.1016/j.jhazmat.2009.04.092

Jiao J, Zhao J, Pei Y (2017) Adsorption of Co (II) from aqueous solutions by water treatment residuals. J Environ Sci 52:232–239

Karthik C, Barathi S, Pugazhendhi A, Ramkumar VS, Thi NBD, Arulselvi PI (2017) Evaluation of Cr(VI) reduction mechanism and removal by *Cellulosimicrobium funkei* strain AR8, a novel haloalkaliphilic bacterium. J Hazard Mater 333:42–53. https://doi.org/10.1016/j.jhazmat.2017.03.037

Keeley J, Jarvis P, Judd SJ (2014) Coagulant recovery from water treatment residuals: a review of applicable technologies. Crit Rev Environ Sci Technol 44:2675–2719

Khan SA, Khan MA (1995) Adsorption of chromium (III), chromium (VI) and silver (I) on bentonite. Waste Manag 15:271–282

Khan TA, Singh VV (2010) Removal of cadmium(II), lead(II), and chromium(VI) ions from aqueous solution using clay. Toxicol Environ Chem 92:1435–1446. https://doi.org/10.1080/02772241003592930

Kim SA et al (2013) Removal of Pb(II) from aqueous solution by a zeolite–nanoscale zero-valent iron composite. Chem Eng J 217:54–60. https://doi.org/10.1016/j.cej.2012.11.097

Klute A, Page AL (1986) Methods of soil analysis. Part 1. Physical and mineralogical methods; Part 2 Chemical and microbiological properties. American Society of Agronomy Inc, New York

Kumari M, Pittman CU, Mohan D (2015) Heavy metals [chromium (VI) and lead (II)] removal from water using mesoporous magnetite (Fe_3O_4) nanospheres. J Colloid Interface Sci 442:120–132. https://doi.org/10.1016/j.jcis.2014.09.012

León-Torres A, Cuerda-Correa EM, Fernández-González C, Alexandre Franco MF, Gómez-Serrano V (2012) On the use of a natural peat for the removal of Cr(VI) from aqueous solutions. J Colloid Interface Sci 386:325–332. https://doi.org/10.1016/j.jcis.2012.07.038

Li Z, Pan Z, Wang Y (2019) Enhanced adsorption of cationic Pb(II) and anionic Cr(VI) ions in aqueous solution by amino-modified nano-sized illite-smectite clay. Environ Sci Pollut Res 26:11126–11139. https://doi.org/10.1007/s11356-019-04447-0

Liu J, Mwamulima T, Wang Y, Fang Y, Song S, Peng C (2017a) Removal of Pb(II) and Cr(VI) from aqueous solutions using the fly ash-based adsorbent material-supported zero-valent iron. J Mol Liq 243:205–211. https://doi.org/10.1016/j.molliq.2017.08.004

Liu Y, Li M, He C (2017b) Removal of Cr(VI) and Hg(II) ions from wastewater by novel β-CD/MGO-SO3H composite. Colloids Surf A 512:129–136. https://doi.org/10.1016/j.colsurfa.2016.10.025

Luo S, Qin P, Shao J, Peng L, Zeng Q, Gu J-D (2013) Synthesis of reactive nanoscale zero valent iron using rectorite supports and its application for Orange II removal. Chem Eng J 223:1–7. https://doi.org/10.1016/j.cej.2012.10.088

Luo W, Fukumori T, Guo B, Osseo-Asare K, Hirajima T, Sasaki K (2017) Effects of grinding montmorillonite and illite on their modification by dioctadecyl dimethyl ammonium chloride and adsorption of perchlorate. Appl Clay Sci 146:325–333. https://doi.org/10.1016/j.clay.2017.06.025

Ma H-L, Zhang Y, Hu Q-H, Yan D, Yu Z-Z, Zhai M (2012) Chemical reduction and removal of Cr(vi) from acidic aqueous solution by ethylenediamine-reduced graphene oxide. J Mater Chem 22:5914–5916. https://doi.org/10.1039/c2jm00145d

Meng L, Chan Y, Wang H, Dai Y, Wang X, Zou J (2016) Recycling of iron and silicon from drinking water treatment sludge for synthesis of magnetic iron oxide@ SiO_2 composites. Environ Sci Pollut Res 23:5122–5133. https://doi.org/10.1007/s11356-015-5742-6

Mondal P, Anweshan A, Purkait MK (2020) Green synthesis and environmental application of iron-based nanomaterials and nanocomposite: a review. Chemosphere 259:127509

Moreira MA et al (2017) Effect of chemical modification of palygorskite and sepiolite by 3-aminopropyltriethoxisilane on adsorption of cationic and anionic dyes. Appl Clay Sci 135:394–404. https://doi.org/10.1016/j.clay.2016.10.022

Naseem R, Tahir SS (2001) Removal of Pb(II) from aqueous/acidic solutions by using bentonite as an adsorbent. Water Res 35:3982–3986. https://doi.org/10.1016/S0043-1354(01)00130-0

Oskui FN, Aghdasinia H, Sorkhabi MG (2019) Adsorption of Cr(III) using an Iranian natural nanoclay: applicable to tannery wastewater: equilibrium, kinetic, and thermodynamic. Environ Earth Sci 78:106. https://doi.org/10.1007/s12665-019-8104-8

Quirantes-Piné R, Funes L, Micol V, Segura-Carretero A, Fernández-Gutiérrez A (2009) High-performance liquid chromatography with diode array detection coupled to electrospray time-of-flight and ion-trap tandem mass spectrometry to identify phenolic compounds from a lemon verbena extract. J Chromatogr A 1216:5391–5397

Saha B, Orvig C (2010) Biosorbents for hexavalent chromium elimination from industrial and municipal effluents. Coord Chem Rev 254:2959–2972. https://doi.org/10.1016/j.ccr.2010.06.005

Sarı A, Tuzen M, Soylak M (2007) Adsorption of Pb(II) and Cr(III) from aqueous solution on Celtek clay. J Hazard Mater 144:41–46. https://doi.org/10.1016/j.jhazmat.2006.09.080

Sedighi H, Irannajad M, Gharabaghi M (2013) Silica impurities removal on bentonite sample for nanoclay production. Amirkabir J Sci Res (AJSR-CEE) 45:11–13

Shanmugharaj AM, Rhee KY, Ryu SH (2006) Influence of dispersing medium on grafting of aminopropyltriethoxysilane in swelling clay materials. J Colloid Interface Sci 298:854–859. https://doi.org/10.1016/j.jcis.2005.12.049

Sharma RK, Puri A, Monga Y, Adholeya A (2014) Acetoacetanilide-functionalized Fe_3O_4 nanoparticles for selective and cyclic removal of Pb2+ ions from different charged wastewaters. J Mater Chem A 2:12888–12898. https://doi.org/10.1039/c4ta01815j

Sharma A, Thakur KK, Mehta P, Pathania D (2018) Efficient adsorption of chlorpheniramine and hexavalent chromium (Cr(VI)) from water system using agronomic waste material. Sustain Chem Pharm 9:1–11. https://doi.org/10.1016/j.scp.2018.04.002

Shi L-n, Lin Y-M, Zhang X, Chen Z-l (2011) Synthesis, characterization and kinetics of bentonite supported nZVI for the removal of Cr(VI) from aqueous solution. Chem Eng J 171:612–617. https://doi.org/10.1016/j.cej.2011.04.038

Sis H, Uysal T (2014) Removal of heavy metal ions from aqueous medium using Kuluncak (Malatya) vermiculites and effect of precipitation on removal. Appl Clay Sci 95:1–8. https://doi.org/10.1016/j.clay.2014.03.018

Şölener M, Tunali S, Özcan AS, Özcan A, Gedikbey T (2008) Adsorption characteristics of lead(II) ions onto the clay/poly(methoxyethyl)acrylamide (PMEA) composite from aqueous solutions. Desalination 223:308–322. https://doi.org/10.1016/j.desal.2007.01.221

Subbaiah MV, Kim D-S (2016) Adsorption of methyl orange from aqueous solution by aminated pumpkin seed powder: kinetics, isotherms, and thermodynamic studies. Ecotoxicol Environ Saf 128:109–117. https://doi.org/10.1016/j.ecoenv.2016.02.016

Suraj G, Iyer CSP, Rugmini S, Lalithambika M (1997) The effect of micronization on kaolinites and their sorption behaviour. Appl Clay Sci 12:111–130. https://doi.org/10.1016/S0169-1317(96)00044-0

Tandon PK, Shukla RC, Singh SB (2013) Removal of Arsenic(III) from water with clay-supported zerovalent iron nanoparticles synthesized with the help of tea liquor. Ind Eng Chem Res 52:10052–10058. https://doi.org/10.1021/ie400702k

Toli A, Chalastara K, Mystrioti C, Xenidis A, Papassiopi N (2016) Incorporation of zero valent iron nanoparticles in the matrix of cationic resin beads for the remediation of Cr(VI) contaminated waters. Environ Pollut 214:419–429

Tyagi B, Chudasama CD, Jasra RV (2006) Determination of structural modification in acid activated montmorillonite clay by FT-IR spectroscopy. Spectrochim Acta Part A Mol Biomol Spectrosc 64:273–278. https://doi.org/10.1016/j.saa.2005.07.018

Wamba AGN et al (2017) Synthesis of grafted natural pozzolan with 3-aminopropyltriethoxysilane: preparation, characterization, and application for removal of Brilliant Green 1 and Reactive Black 5 from aqueous solutions. Environ Sci Pollut Res 24:21807–21820. https://doi.org/10.1007/s11356-017-9825-4

Yadav S, Srivastava V, Banerjee S, Weng C-H, Sharma YC (2013) Adsorption characteristics of modified sand for the removal of hexavalent chromium ions from aqueous solutions: kinetic, thermodynamic and equilibrium studies. CATENA 100:120–127. https://doi.org/10.1016/j.catena.2012.08.002

Yadava KP, Tyagi BS, Singh VN (1991) Effect of temperature on the removal of lead(II) by adsorption on China clay and wollastonite. J Chem Technol Biotechnol 51:47–60. https://doi.org/10.1002/jctb.280510105

Yang J et al (2019) Nanomaterials for the removal of heavy metals from wastewater. Nanomaterials 9:424

Yazdani M, Ebrahimi-Nik M, Heidari A, Abbaspour-Fard MH (2019) Improvement of biogas production from slaughterhouse wastewater using biosynthesized iron nanoparticles from water treatment sludge. Renew Energy 135:496–501. https://doi.org/10.1016/j.renene.2018.12.019

Yuan P et al (2009) Montmorillonite-supported magnetite nanoparticles for the removal of hexavalent chromium [Cr(VI)] from aqueous solutions. J Hazard Mater 166:821–829. https://doi.org/10.1016/j.jhazmat.2008.11.083

Yuan P et al (2010) Removal of hexavalent chromium [Cr(VI)] from aqueous solutions by the diatomite-supported/unsupported magnetite nanoparticles. J Hazard Mater 173:614–621

Yuan GD, Theng BKG, Churchman GJ, Gates WP (2013) Chapter Clays and Clay Minerals for Pollution Control. In: Bergaya F, Lagaly G (eds) Developments in clay science, vol 5. Elsevier, Amsterdam, pp 587–644. https://doi.org/10.1016/B978-0-08-098259-5.00021-4

Zhang X, Lin S, Chen Z, Megharaj M, Naidu R (2011) Kaolinite-supported nanoscale zero-valent iron for removal of Pb2+ from aqueous solution: reactivity, characterization and mechanism. Water Res 45:3481–3488. https://doi.org/10.1016/j.watres.2011.04.010

Zhang Y-Y, Jiang H, Zhang Y, Xie J-F (2013) The dispersity-dependent interaction between montmorillonite supported nZVI and Cr(VI) in aqueous solution. Chem Eng J 229:412–419. https://doi.org/10.1016/j.cej.2013.06.031

Zhang S-H et al (2018) Mechanism investigation of anoxic Cr(VI) removal by nano zero-valent iron based on XPS analysis in time scale. Chem Eng J 335:945–953

Zhang Y, Jiao X, Liu N, Lv J, Yang Y (2020) Enhanced removal of aqueous Cr(VI) by a green synthesized nanoscale zero-valent iron supported on oak wood biochar. Chemosphere 245:125542. https://doi.org/10.1016/j.chemosphere.2019.125542

Zhao YQ, Doherty LP, Doyle D (2011) Fate of water treatment residual: an entire profile of Ireland regarding beneficial reuse. Int J Environ Stud 68:161–170. https://doi.org/10.1080/00207233.2010.543564

Zhou Z et al (2018) Optimized removal of natural organic matter by ultrasound-assisted coagulation of recycling drinking water

treatment sludge. Ultrason Sonochem 48:171–180. https://doi.org/10.1016/j.ultsonch.2018.05.022

Zhu S et al (2015) A novel conversion of the groundwater treatment sludge to magnetic particles for the adsorption of methylene blue. J Hazard Mater 292:173–179. https://doi.org/10.1016/j.jhazmat.2015.03.028

Zhu F, Ma S, Liu T, Deng X (2018a) Green synthesis of nano zero-valent iron/Cu by green tea to remove hexavalent chromium from groundwater. J Clean Prod 174:184–190

Zhu S et al (2018b) Hydrothermal synthesis of a magnetic adsorbent from wasted iron mud for effective removal of heavy metals from smelting wastewater. Environ Sci Pollut Res 25:22710–22724

Zou J et al (2012) Structure and properties of noncrystalline nano-$Al(OH)_3$ reclaimed from carbonized residual wastewater treatment sludge. Environ Sci Technol 46:4560–4566

Zou J et al (2013) Recovery of silicon from sewage sludge for production of high-purity nano-SiO_2. Chemosphere 90:2332–2339